ELSEVIER

Synthetically tunable polymers, free volume element size distributions, and dielectric breakdown field strengths

Sebastian M. Fica-Contreras [1], Zongze Li [2], Abdullah Alamri [3], Aaron P. Charnay [1], Junkun Pan [1], Chao Wu [2], Jeffrey R. Lockwood [4], Omer Yassin [4], Stuti Shukla [4], Gregory Sotzing [3,4], Yang Cao [2], Michael D. Fayer [1,*]

[1] Department of Chemistry, Stanford University, Stanford, CA 94305, United States
[2] Department of Electrical and Computer Engineering, University of Connecticut, Storrs, CT 06269, United States
[3] Institute of Materials Science, University of Connecticut, Storrs, CT 06269, United States
[4] Department of Chemistry, University of Connecticut, Storrs, CT, 06269, United States

Four polyetherimide (PEI) polymers were synthesized with different end groups, while leaving the molecular weights, glass transition temperature, thermal properties, and dielectric constant essentially unchanged. The Restricted Orientation Anisotropy Method (ROAM), an ultrafast infrared laser technique, was used to measure the films' free volume elements (FVEs) radius probability distribution (RPD) curves. This technique exploits the observation that a vibrational probe's molecular reorientation dynamics inside a polymer film's FVEs are sterically restricted by the surfaces of the FVEs. The measured RPD curves displayed significant changes in shape and center positions for the PEI polymers with different end cap. The results demonstrate that structural changes to the end groups of a polymer can significantly modify its microscopic morphology, which is consistent with other experiments that observed changes in macroscopic observables. The thin film samples' breakdown fields (E_{BD}) were measured, and a correlation between polymer films having a higher probability of large FVEs and lower E_{BD}s was observed. This work demonstrates that the nanoscopic chain packing structure that controls the nature of the FVEs and breakdown field properties of PEI are synthetically tunable, without the need to change the main chain chemical structure. The results provide some experimental evidence for the theoretical model of electron-acceleration inside FVEs as the microscopic origin of polymer film dielectric breakdown. The results also provide a framework for the study of other polymer dielectrics, and suggest that design of high breakdown field polymer films may involve minimizing FVE sizes, particularly the large FVE tails of the size distribution.

Keywords: Polyetherimide; Dielectric breakdown; Polymer free volume; Ultrafast infrared spectroscopy

Introduction

Polymeric free volume is responsible for many macroscopic material characteristics such as thermal response [1,2], viscosity [3], gas permeability [4,84], and transport properties [5,6]. As a polymer film crosses below its glass transition temperature, T_g, the density of the material increases and chain mobility is vastly

* Corresponding author.
E-mail addresses: Sotzing, Gregory (g.sotzing@uconn.edu), Cao, Y. (yang.cao@uconn.edu), Fayer, M.D. (fayer@stanford.edu).

 https://doi.org/10.1016/j.mattod.2023.05.010

diminished [4,7,8], locking the polymer chains in a high-energy, non-equilibrium configuration [4]. This state is characterized by inefficient packing [4,9,10] and minimal segmental mobility [11], which leaves a series of pockets of unoccupied space of different structures and sizes (several angstroms in radius), called free volume elements (FVEs) [12,13], scattered throughout the matrix. The total percent of unoccupied volume of a polymer is referred to as the fractional free volume (FFV) [14]. FVEs, on the other hand, represent only a portion of the film's FFV [12,15,16] and can be thought of as a specific important type of free volume. Collectively, FVEs are partly responsible for the structural heterogeneity that is characteristic of polymeric materials [17].

One important property of polymer films is their behavior as dielectrics in capacitors [18]. Some desirable characteristics of dielectrics are high polarizability, high dielectric constant, low dielectric loss, good thermal stability, malleability, and high dielectric breakdown field [18–20]. Ceramics provide high dielectric constants, if linear, and remarkable thermal stability, but suffer from poor flexibility and low, non-graceful breakdown strengths, which result in low energy densities [18,21,22]. Polymer dielectrics, conversely, are lightweight, synthetically tunable, easily processed, and have higher breakdown strength [18,21,23]. Moreover, novel organic synthetic techniques provide a vast library of polymer structures and characteristics. Hence, the rational design of polymers drives many research efforts to develop structures that are versatile dielectrics [24–26].

All dielectric materials have an external electric field upper strength limit, called the dielectric breakdown field, E_{BD} [27], above which they become electrically conducting, i.e., dielectric breakdown [28,29]. This parameter is fundamental in determining a polymer's dielectric performance as an insulator, gate dielectric, and capacitor dielectric for electrical and electronic applications [30–33]. However, to date, complete understanding of the relevant factors or mechanisms that govern breakdown does not exist [30,32–34].

There are two types of dielectric breakdown. In intrinsic breakdown processes, the E_{BD} is determined solely by the electronic structure of the pristine polymer [27,28], and it is most relevant for pulsed system applications where the material is subjected to high peak power and *E*-fields near its breaking point [27,35]. By contrast, although related, extrinsic breakdown occurs over macroscopic timescales (up to decades) [27,35,36], and it results from aging as well as from field-induced polymer degradation, which cause the accumulation of structural defects and charge carriers that lower a polymer film's dielectric strength [37]. In this work, we examine intrinsic breakdown and its relation to a film's microscopic structure.

Dielectric breakdown results from a complicated interplay of electronic, mechanical, and thermal properties. Understanding breakdown is made more complex by polymers' molecular-level topological disorder. Although the connection between microscopic polymer structure and macroscopic dielectric properties has been recognized [38–41], a detailed understanding of the mechanistic and structural factors that determine these material properties is lacking. One hypothesis is that a polymer film's E_{BD} is, at least partially, determined by the sizes of its FVEs [42], as they alter the polymer's ability for energy storage, i.e., energy density, and/or its energy discharge efficiency under a high electric field [25]. A theory that tries to quantitatively relate free volume element sizes to dielectric breakdown was proposed by Artbauer in 1996 [42]. This model and its relation to our results is discussed below.

Because it is well-known that introducing structural modifications to a polymer chain leads to significant changes in the FVE sizes of the matrix [43–50], simultaneously measuring free volume and breakdown fields of synthetically modified polymer structures is a promising approach to obtaining a systematic view of the relationship between these two quantities. Specifically, this work seeks to identify a connection between the FVE radius probability distribution of a polymer film and its E_{BD} by studying a series of synthetically modified PEI films.

The Restricted Orientation Anisotropy Method (ROAM) was used to measure FVE size distributions. ROAM has the ability to extract a film's FVE radii, radius probability distribution (RPD), and intrinsic FVE size-dependent electric fields from an ultrafast infrared pump–probe spectroscopy experiment [51].

Polyetherimide (PEI) is a high-quality dielectric with a high breakdown field of ~500 MV/m. PEI is amenable to structural modifications via organic synthesis, and because of its amorphous nature, it can be solvent cast into thin films [52–57]. Possessing good thermal stability and a well-balanced band gap [58,59], PEI is useful for high temperature and high field applications.

PEI was modified by introducing a series of mono aromatic and aliphatic amine end caps that systematically increase the volume of the end-group. End capping is a popular method to control polymer properties like molecular weight or mechanical, electrical, optical properties, and gas permeation [39,40,60–64]. Changing the end groups introduces only a small structural perturbation of the polymer, while maintaining the bulk of the molecule and its electronic structure intact. The molecules used for this purpose were *p*-toluidine, 4-*tert*-butylaniline, 1-adamantylamine, and 2,4,6-tri-*tert*-butylaniline. The end groups were chosen based on their molecular volume and ease of rotation. *p*-Toluidine is less volume filling than 4-*tert*-butylaniline, yet they have a similar rotational energy barrier, whereas both 1-adamantylamine and 2,4,6-tri-*tert*-butylaniline occupy a larger volume than *p*-toluidine and 4-*tert*-butylaniline. The 1-adamantyl group has the same number of carbon atoms as the *tert*-butylbenzene group, yet one less degree of unsaturation, and would occupy approximately the same molecular volume. However, unlike *tert*-butylbenzene, due to its geometry, rotation of the adamantyl group should not displace its occupied volume. The 2,4,6-tri-*tert*-butylaniline end group has two additional *t*-butyl substituents, which introduce eight additional carbon atoms and make it the largest of the end groups. As such, the rotation of this end group should experience the largest extent of restriction. The degree of end group rotation will be linked to the membranes' FVE sizes and dielectric breakdown fields below.

The four end capped polymers were solvent-cast into films, their FVE RPDs extracted, and their E_{BD}s measured. Changing the end cap of PEI significantly changes the center position and width of the FVE radius probability distribution. Additionally, we observed a relationship between the probability of having large FVEs and lowering a film's dielectric breakdown field.

Together, these results provide insights into the microscopic origin of polymer dielectric breakdown and suggest that increasing the packing efficiency of a polymer film, i.e., reducing the probability of large FVEs, is a viable way of increasing its breakdown field.

Experimental methods

Polymer synthesis

All reagents were used as received without further purification unless otherwise specified. 4,4-bisphenol A dianhydride (BisDA) was provided by SABIC, and *m*-phenylenediamine and *m*-cresol were purchased from Across Organics. 4-*tert*-Butylaniline, 2,4,6-tri-*tert*-butylaniline, 1-adamantylamine, and *p*-toluidine were purchased from Oakwood Chemicals. Methanol was purchased from Fisher Scientific. BisDA was recrystallized from acetic anhydride. *m*-Cresol was used as the reaction solvent and purified by vacuum distillation before use. Reactions were performed under an inert argon atmosphere.

PEI was prepared by a step polymerization reaction (Scheme 1). A detailed description of the reaction procedures as well as Nuclear Magnetic Resonance (NMR) spectra, Gel Permeation Chromatography (GPC), thermal and electrical characterization of the structures are presented in the Supplemental Information (SI). The chains had ~40 monomer units with narrow dispersion.

With this number of monomers, the end groups represent 5% of the total units per polymer chain, which is a significant percentage. It will be shown below that changing the end groups causes large changes in the films' distributions of FVE radii. Previous studies investigated the effect of end group structure and additive concentration on polymer membranes' gas permeability [64–67], which is a macroscopic property repeatedly linked to polymeric free volume elements. Such studies consistently observed large differences in gas permeability for different end groups and additive concentrations using polymers of similar molecular weight to the ones used here and at similar concentrations, 5% or less.

It is important to highlight that all polymers were synthesized and processed in parallel and following identical experimental procedures, removing all remaining reagents to avoid plasticizing effects to ensure minimal variation across samples other than on the structure of the end groups.

Sample preparation

For the IR measurements, PEI films were prepared in parallel and using the same procedure to avoid artificially introducing differences across films. The density of PEI was used to determine an appropriate mass of polymer to create a 2.5-cm in diameter and 150 μm thick film. The polymer was dissolved in chloroform and phenyl selenocyanate (PhSeCN, the vibration probe) was added. The solution was thoroughly mixed and deposited in a glass container on a level surface. The excess chloroform was allowed to slowly evaporate overnight, leaving behind a solid film of the desired dimensions. The films were heated in a vacuum oven at <100 mTorr with the temperature increased in steps, starting at 100 °C for 1 day, and followed by 1 day at 120 °C, 3 days at 140 °C, and finally 1 day at 160 °C. Due to the thickness of the films, an incremental step drying procedure was used to avoid rapid solvent evaporation, which leads to the formation of bubbles. After drying, a small piece of each film was dissolved in deuterated dichloromethane and quantitative NMR measurements were used to ensure that no chloroform remained in the films (see SI). All samples were stored in a glovebox to avoid atmospheric water uptake by the films.

The linear absorption spectrum of the symmetric CN stretch of PhSeCN was measured with Fourier-Transform Infrared (FT-

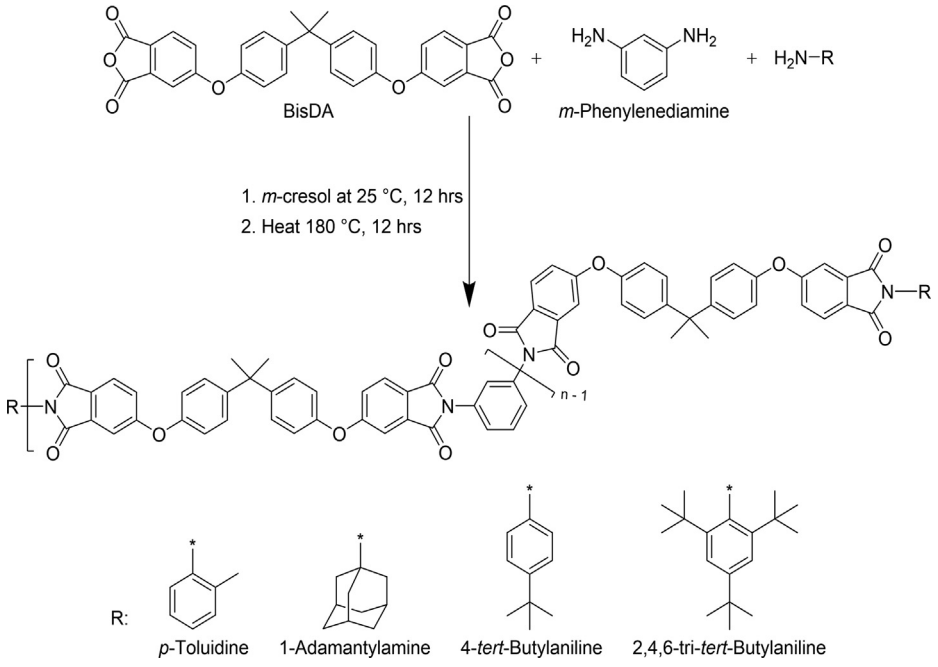

SCHEME 1

Reaction conditions used to synthesize polyetherimide (PEI) structures with different end caps.

IR) Spectroscopy to determine the final concentration of the vibrational probe (epsilon = 51.3 mM cm^{-1}). The orientational dynamics of PhSeCN were measured as a function of probe concentration and at different positions on two films to ensure that the probe did not act as a plasticizer and to ensure sample reproducibility. The concentration of PhSeCN was kept below 300 mM to avoid plasticizing effects. A detailed description of the NMR and FT-IR spectra used to characterize the chemical composition of the films is presented in the SI.

For dielectric measurements, a 13–15% polymer solution was cast to form a 10 μm thick film. The polymer was dissolved in *N*, *N*-dimethylacetamide (DEMAc), and after complete solvation, the solution was passed through a 45-μm microfilter to remove any undissolved material. The filtered solution was cast on a glass substrate at 60 °C for two hours and the film was kept drying overnight at room temperature. Deionized water was used to peel the film off the glass substrate. The film was dried in a vacuum oven at 140 °C for four days to remove residual solvent and water.

Breakdown measurements

The breakdown strength was measured with the voltage ramping at a rate of 300 V/s using ball-plate electrodes until breakdown occurred. All polymer films were tested with multiple specimens to generate more than ten breakdown data points for Weibull statistics. The characteristic breakdown values at 63.2% (1–1/e) probability of failure are used as the breakdown strength of each polymer and the error bars were estimated using a 90% confidence interval. The samples are free-standing films, of ~10 μm uniform thickness and of area larger than 5 by 5 cm to avoid surface flashover. The surfaces of the films were flat and smooth, and the films were free of particulates and pinholes.

Fourier Transformed Infrared (FT-IR) spectroscopy

Each film was placed in a copper sample cell holder between two calcium fluoride (CaF_2) windows. The linear infrared absorption spectrum of the CN stretch of PhSeCN in each PEI film was collected using a resolution of 0.24 cm^{-1}. Background subtraction was performed by collecting the probe-free absorption spectrum of PEI and subtracting it from the sample with the probe. FT-IR spectra of the CN stretch of PhSeCN in four different end capped PEI films are shown in Fig. 1. The linear absorption spectra are discussed in detail below.

Polarization-Selective Pump-Probe (PSPP) spectroscopy

Only a brief description of the instrumentation is given here because a detailed description of an analogous instrument has been provided previously [68,69]. A Ti:Sapphire oscillator seeding a regenerative amplifier was used to produce 800 nm femtosecond pulses with 2 mJ of energy per pulse and 3 kHz repetition rate. The output from the regenerative amplifier is converted from 800 nm to 4.6 μm (30 μJ and 3 kHz repetition rate) using a home-built optical parametric amplifier (OPA) and difference frequency generation using a silver gallium sulfide (AGS) crystal. The 4.6 μm pulses had a bandwidth of ~100 cm^{-1} and were near transform-limited. The mid-IR OPA output was tuned to be resonant with the vibrational frequency of the symmetric CN stretch of PhSeCN.

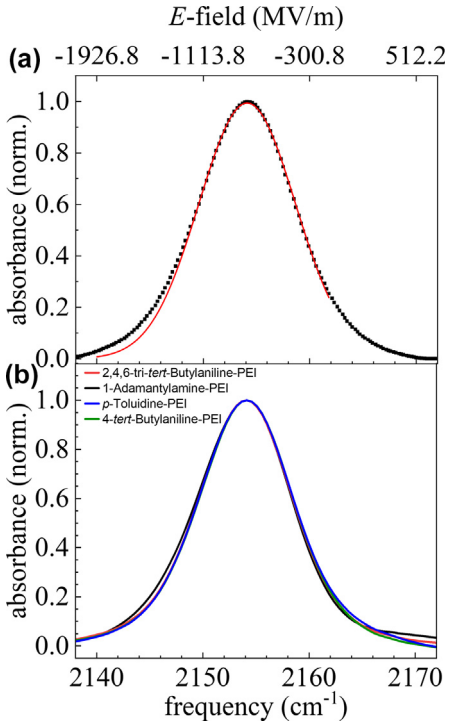

FIG. 1

Absorption spectra of the CN stretch vibrational mode of PhSeCN. (A) Representative spectrum in PEI and (B) four end capped PEI films. The spectra are well characterized by Gaussian functions on the high frequency half, but there is a tail to low frequency. A detailed description of the spectral fits is presented in the SI. No differences are observable in the spectra either in center frequencies or widths, showing that the presence of the end cap does not affect the time-averaged spectrum. The top axis gives the approximate *E*-fields inside the FVEs as a function of frequency.

The IR pulse was split into a strong pump pulse (~90% intensity) and a weak probe pulse (~5% intensity). The pump was directed through a germanium acousto-optic modulator (AOM) for pulse shaping, which is used to block the frequencies of light resonant with the PhSeCN nitrile stretch on every other pump pulse [70] and for phase cycling, which reduces scattered light. The probe was passed down a mechanical delay stage with a delay range of ~2 ns. Before reaching the sample, the polarization of the pump pulse was rotated with a half wave plate and polarizer to +45° relative to the probe pulse. A polarizer on a computer-controlled rotation stage was used to resolve the probe polarization after the sample at +45° and −45°, for parallel and perpendicular measurements relative to the pump polarization, respectively. The pump and probe pulses overlapped in the sample, and their separation in arrival time was precisely controlled with the mechanical delay stage mentioned above. The probe pulse was frequency resolved using a spectrograph and a 32-pixel mercury cadmium telluride (MCT) array detector. An additional horizontal polarizer was placed after the rotating polarizer to match the detected probe intensity in each polarization on the MCT array to eliminate the polarization-dependent diffraction efficiency of the grating in the monochromator. The signal was the difference in transmitted probe intensity between shots with the pump on and shots with the resonant pump blocked. The time evolution of the parallel ($I_{\parallel}$) and perpendicular ($I_{\perp}$) pump–

probe signals was obtained by increasing the time delay, t, between pump and probe pulses.

$I_{||}(t)$ and $I_{\perp}(t)$ were combined using the following equations [71,72]:

$$P(t) = \frac{1}{3}\left(I_{||} + 2I_{\perp}\right)$$
$$r(t) = \left(\frac{I_{||} - I_{\perp}}{I_{||} + 2I_{\perp}}\right) = 0.4C_2(t) \quad (1)$$

where $P(t)$ is the isotropic signal, i.e., the CN vibrational excited-state population lifetime, and $C_2(t)$ is the second Legendre polynomial orientational correlation function. For the current study, the observable of interest is the orientational dynamics of the CN stretch given by the anisotropy decay, $r(t)$.

Restricted Orientation Anisotropy Method (ROAM)

The details of the analyses that follow the PSPP measurement to determine the polymer's FVE radii and FVE radius probability distribution (RPD) using ROAM have been published previously [51] and will only be discussed briefly below.

The following is a very qualitative analogy illustrating how the method works. Imagine you twirl a baton in a room much larger than the length of the baton. The baton will spin all the way around, sampling all angles. Now imagine you take the same baton into a very small room. This time, when you try to twirl the baton, it hits one wall and then the opposite wall, and as a result, it can only move through a limited range of angles. If you know the range of angles and the length of the baton, it is straightforward to calculate the distance between the walls of the small room. In ROAM, the small room is an FVE and the baton is the IR probe molecule. In the context of ROAM, the PSPP experiments measure the range of angles (anisotropy decay) sampled by the vibrational probe, and electronic structure calculations determine the length of the probe molecule. The anisotropy decays vary across the inhomogeneously broadened vibrational probe's IR absorption spectrum. The anisotropy decays and the absorption spectrum are sufficient to obtain the radii of the FVEs and the radius probability distribution.

The anisotropy decay curves, $r(t)$, of PhSeCN in polymers are accurately described by a biexponential decay to a static, nonzero final offset. The orientational dynamics of PhSeCN are analyzed using the well-established wobbling-in-a-cone (WIAC) theory [73–75], and the frequency-dependent anisotropy curves (see Eq. (1)) are parametrized using the following expression:

$$C_2(t) = S_0^2\left(S_1^2 + \left(1 - S_1^2\right)\exp(-t/\tau_1)\right)\left(S_2^2 + \left(1 - S_2^2\right)\exp(-t/\tau_2)\right) \quad (2)$$

In the WIAC model, molecular reorientation results from ranges of angular fluctuations, each described by a cone half-angle, and with each subsequent set of fluctuations spanning a wider range of angular space. The order parameters S_0, S_1, and S_2 (Eq. (2)) describe PhSeCN's angular range of reorientation as it wobbles about its center of mass, and are related to a cone half-angle, θ_i, by:

$$S_i = \frac{1}{2}\cos(\theta_i)(1 + \cos(\theta_i)) \quad (3)$$

where three order parameters, S_0, S_1, S_2, give rise to three cone half-angles: θ_0, θ_1, θ_2. θ_0 is associated with ultrafast (<100 fs) inertial motions, which are too fast to resolve experimentally, whereas θ_1 describes fast diffusive motions that have experimentally measurable time scales, ~10 ps. Although the time dependence of the inertial motions cannot be measured, the half-angles θ_0 can be obtained from the experiments. Both the inertial and fast diffusive motions occur on time scales faster than structural changes of the polymer, such as side group position fluctuations. Therefore, as the cumulative angular space described by θ_0 and θ_1 is determined by the FVE size, it is appropriate to combine these two parameters. The cone half-angle given by S_0S_1, provides θ_{0+1}, which describes the cone half-angle associated with the size of the FVE. θ_{0+1} displays a strong frequency dependence, with a tendency to converge as the frequency decreases.

While the values of θ_{0+1} are sampled faster than molecular motions, and are used to determine the FVE sizes as a function of frequency, θ_2, which is obtained from the second, slower exponential component of $r(t)$, provides other important information that has been discussed previously [51]. The slow exponential arises from shape and center position fluctuations of the FVEs. While at a given frequency the ensemble average size does not change with time, motions of side groups and small chain segmental motions cause the shape and center positions of FVEs to fluctuate. Such fluctuations can be important, as they will cause the separation of nearby FVEs to change with time on a ~150 ps time scale. In this work, we only focus on the differences in θ_{0+1} as a function of PEI end group.

Full molecular reorientation, e.g., a probe molecule in a liquid, results in a complete decay of the anisotropy to zero, as the probe molecule samples all orientations (angles). In a low viscosity liquid, complete reorientation will be fast, while in a high viscosity liquid it will be slow. In polymers, the PhSeCN probe molecules are located in FVEs, which are too small for the probes to undergo complete orientational randomization. As a result, the probe can sample a range of angles, but then hits the wall of the FVE, preventing complete angular sampling. The result of restricted angular sampling is the anisotropy decays to a non-zero offset. However, it is θ_{0+1} at each frequency that result from a different FVE size. The data analysis separates θ_{0+1} from θ_2 and the final offset. By determining the molecular dimensions of the probe and the range of angles from the WIAC theory, the cumulative cone-half angles, θ_{0+1}, are related to the radius of a cylindrical element by,

$$r_i = a\sin\theta_i + \Delta r \quad (4)$$

where r_i is the FVE radius, θ_i is the range of angles sampled, Δr is the radius of the molecular moiety that collides with the inner wall of the FVE, and a is the distance between PhSeCN's center of mass and the center of the moiety that impacts the FVE wall [51,76].

The first-order Stark effect causes the vibrational frequency of the CN stretch in PhSeCN to depend on the electric field created by the surrounding environment [77–79]. Nitriles have a large first order Stark effect, and methods to characterize a particular molecule's Stark tuning rate (frequency shift as a function of electric field) are well established. A distribution of FVE sizes results in an inhomogeneous distribution of chemical environments, producing a range of electric fields and vibrational frequencies. Thus, the CN stretch of PhSeCN has an inhomogeneously broadened linear absorption spectrum (Fig. 1). Each frequency dependent anisotropy curve in the PSPP experiment provides the

orientational dynamics of PhSeCN in a particular subensemble of environments that have a specific average FVE radius. Since the anisotropy decays are frequency dependent, the WIAC model provides a series of frequency-dependent cone angles (Eq. (3), which result in a series of frequency-dependent FVE radii (Eq. (4), Fig. 3).

The PPSP experiments yield the FVE radii as a function of frequency. The linear absorption spectrum is related to the probability of having a particular frequency. Combining these two experimental results, the polymer's radius probability distribution (RPD) curve is obtained using Bayes' theorem and a maximum entropy mathematical formalism [51]. The experimentally measured FVE radii are expressed as the following expectation value:

$$\langle r(\omega)\rangle = \frac{1}{\rho(\omega)}\int_0^\infty \rho(\omega|r)\rho(r)r dr \quad (5)$$

where $\rho(\omega|r)$ is the conditional probability density function (PDF) that a probe having frequency ω is in an FVE of radius r. $\rho(r)$ is the probability of having an FVE of radius r (quantity of interest), and $\rho(\omega)$ is the area-normalized linear absorption spectrum of the vibrational probe. $\rho(\omega|r)$ and $\rho(r)$ are iterated to simultaneously reproduce two fundamentally different experimental observables, $\rho(\omega)$ (the absorption spectrum) and $\langle r(\omega)\rangle$ (the measured FVE radii as a function of frequency). The requirement to simultaneously reproduce both observables greatly constrains the resulting $\rho(r)$.

Results and discussion

Fig. 1 shows the absorption spectra of the symmetric CN stretch of PhSeCN in four end capped PEI films. A representative spectrum is shown in Fig. 1A. A Gaussian function fit was used to obtain the center frequency and full width at half maximum (FWHM) of each absorption line. The fits were performed on the high frequency half of the spectra and extended to lower frequency. The results of fits to all the spectra, shown in Fig. 1B, are presented in the SI. The absorption line in the low frequency regime is not Gaussian, i.e., it displays a tail. The vibrational lifetime is a single exponential decay across the entire spectrum, which demonstrates that the tail does not arise from a distinct ensemble of probe molecules. Therefore, as discussed previously, the non-Gaussian line shapes result from a non-Gaussian distribution of local chemical environments, i.e., FVE sizes [51], which will be discussed below when the FVE radius probability distribution curves are presented. In Fig. 1B it is evident that the probe spectra from the end capped PEI films are identical within experimental error, which is caused mainly by background subtraction. All spectra are centered at 2154 cm^{-1} and have a FWHM of ~10 cm^{-1}. These parameters are consistent with previous reports of the vibrational frequency of the CN stretch in PhSeCN [79]. While the FT-IR spectra are identical, it will be seen below that the microscopic structure of the polymer films, as elucidated via the measurement of time dependent probe dynamics, differ significantly.

Fig. 2 displays the orientational dynamics of PhSeCN in 1-adamantylamine-PEI. Only one orientational dynamics data set is presented here to illustrate the main features of the results. The data and a detailed description of the orientational dynamics in other films are presented in the SI. The anisotropy decays are

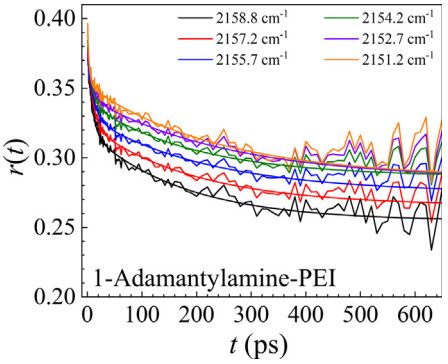

FIG. 2

Orientational relaxation data of PhSeCN in a 1-adamantylamine-PEI film. The orientational relaxation is a biexponential decay to a constant at long time (solid lines). The data display a strong frequency dependence, with a greater extent of decay with increasing frequency. The orientational dynamics curves tend to converge in the low frequency regime and spread in the high frequency regime.

characterized by a strong frequency dependence in all samples. As discussed above, the frequency of a vibrational probe is partially determined by the surrounding local chemical environment. Therefore, each curve represents the orientational dynamics of a sub-ensemble of probes in a different polymer environment, i.e., FVE size. The curves are accurately fit with a frequency-dependent biexponential decay to a non-zero offset. An anisotropy curve has a maximum value of 0.4 (Eq. (1)) and a minimum possible value of zero, which correspond to having no molecular reorientation and full reorientation, respectively. The non-zero final offset demonstrates that the molecular reorientation of the probe is restricted, such that the probe can only sample a finite range of angles. Because the extent of the anisotropy decay is frequency dependent, the results for distinct frequencies reflect that different sub-ensembles of vibrational probes have their molecular reorientation restricted to different extents. The data that are important for this study are the fast decays on the ~10 ps time scale. As the frequency in the absorption spectrum of the sub-ensemble increases, so does the extent of decay, which indicates that there is less restriction to the fast molecular reorientation, i.e., larger FVEs, with increasing vibrational frequency. The decays also tend towards convergence in the low frequency regime; an effect that is related to the non-Gaussian profile of the RPD curves [51] presented and discussed below.

The important result of this work is that the orientational dynamics of PhSeCN are different for different PEI films (see SI), and as discussed below, so are the E_{BD}s. These results show that a subtle structural change to the end groups of a polymer, which leaves most of the polymer chain intact, causes a significant change in the orientational dynamics of an embedded vibration probe. As shown below, the change in orientational dynamics results from different FVE radius probability distributions.

The frequency dependent FVE radii extracted from the orientational dynamics using Eqs. (2)–(4) for the four PEI film samples are presented in Fig. 3. The dashed curves are included as guides to the eye so the differences between the samples can be seen

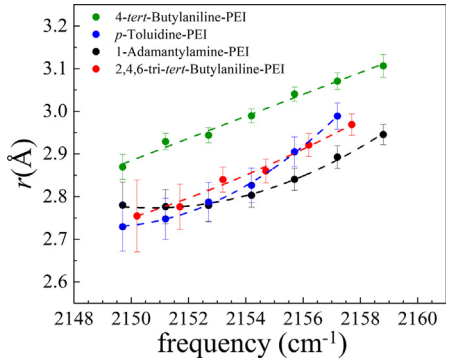

FIG. 3

Frequency dependent FVE radii of four end-capped PEI films. The FVE radius increases with increasing vibrational frequency of the probe. Two regimes are observed: the FVE radii in 4-*tert*-butylaniline-PEI are larger, whereas the FVEs in all other films are smaller. The dashed lines are guides to the eye.

clearly. These FVEs correspond to vibrational frequencies of a range that is approximately the FWHM of the absorption spectra (see Fig. 1). The FVEs have radii that span the range between 2.70 and 3.05 Å. These values are consistent with other reports of the typical sizes of polymer FVEs obtained from positron annihilation lifetime spectroscopy (PALS) [80–83]. An in-depth comparison of ROAM to PALS has been published, in which the methods and assumptions, as well as their effect on the observed results, are discussed [51].

Two main regimes are observed: the 4-*tert*-butylaniline end cap displays FVEs in the range between 2.85 and 3.05 Å. In contrast, *p*-toluidine, 1-adamantylamine, and 2,4,6-tri-*tert*-butylaniline all cause the PEI FVEs to become smaller than in the 4-*tert*-butylaniline-PEI film (between 2.7 and 2.9 Å). While 2,4,6-tri-*tert*-butylaniline displays a close to linear dependence of the FVE radii with respect to frequency across the entire frequency range, 1-adamantylamine, and to a lesser extent *p*-toluidine, display a linear dependence only at high frequency, but the FVE radii converge toward a single value at low frequency. This effect results directly from the similarity of the low frequency orientational dynamics (Fig. 2). This behavior has been observed in polystyrene and poly(methyl methacrylate) before, and it indicates that the FVE RPD is non-Gaussian (see below) [51]. ROAM does not assume a functional form for the distribution of FVE sizes. Substantial deviations from Gaussian RPDs can be observed, which will be important below when the relation between RPD curves and breakdown fields is discussed.

Fig. 4A displays the RPD curves obtained for the four PEI samples with different end caps. The details of the mathematical formalism involved in the extraction of these curves has been published previously [83], and associated results are presented in the SI. 2,4,6-tri-*tert*-butylaniline-PEI has a Gaussian distribution of FVE radii within experimental error. By contrast, the other three end capped samples have non-Gaussian RPDs, with tails that extend to larger FVE radii. The tail is subtle in 4-*tert*-butylaniline-PEI, and more pronounced in 1-adamantylamine-PEI and *p*-toluidine-PEI. All except 4-*tert*-butylaniline-PEI curves have essentially non-zero probability starting in the range between 2.25 and 2.4 Å. Only 4-*tert*-butylaniline-PEI has non-

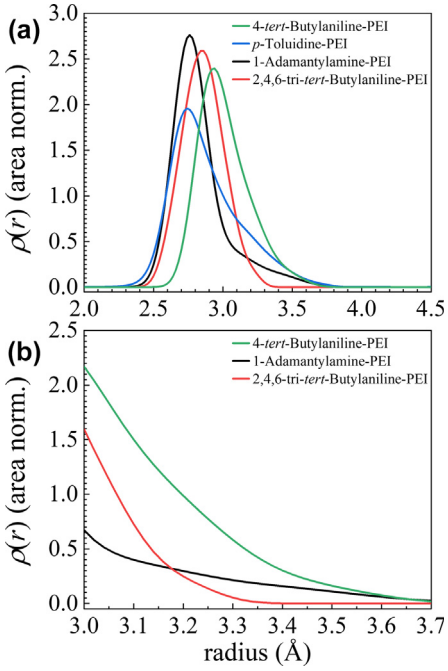

FIG. 4

FVE radius probability distribution (RPD) curves in four end capped PEI films (A). The probability curves are area normalized to highlight differences in the line shapes. The RPD curve of 2,4,6-tri-*tert*-butylaniline-PEI has a close to Gaussian line shape, but the others are highly non-Gaussian with long tails to large radii. (B) A blow up of the large radius portion of the plots in A. The films' amplitudes in the tails of the distributions are correlated with their breakdown field.

zero amplitude starting at 2.6 Å. The RPD curves extend to 3.7 Å, with the only exception 2,4,6-tri-*tert*-butylaniline-PEI, which extends to only 3.35 Å. The maxima of these curves, in increasing order, are *p*-toluidine-PEI (2.74 Å), 1-adamantylamine-PEI (2.76 Å), 2,4,6-tri-*tert*-butylaniline-PEI (2.85 Å), and 4-*tert*-butylaniline-PEI (2.94 Å). The maximum FVE radii and FWHMs of each curve are summarized in Table 1.

Before exploring these observations further, it is important to emphasize that these results demonstrate that modifying the structure of the end groups of a polymer not only can shift the absolute size of the FVE RPD, but it can also substantially change the shape and width of the FVE size distribution. The results show that small structural changes can significantly influence the distribution of FVE sizes even while keeping the bulk of the structure intact and without the need for co-polymerization, branching, or the addition of plasticizers [43–45], at least for these relatively short chains. Modification of the polymer nanoscopic structure without significantly changing the chemical nature of the material is central to this study. Changing only the end groups eliminates significant electronic structure changes of the chains. Moreover, because ROAM can measure absolute FVE sizes and radius probability distributions, these modified PEIs permit a direct correlation between FVE sizes and macroscopic polymeric properties, i.e., dielectric characteristics, while keeping the main polymer chain unchanged.

Table 1 summarizes the E_{BD} values obtained for the four PEI thin film samples. A thin film of *p*-toluidine-PEI could not be made with sufficient quality for breakdown testing. The highest

E_{BD} was obtained for 2,4,6-tri-*tert*-butylaniline-PEI with 467 MV/m, followed by 1-adamantylamine-PEI with 429 MV/m, and then by 4-*tert*-butylaniline-PEI with 392 MV/m. The breakdown field of the laboratory-made PEI films is low compared to the usually quoted 500 MV/m for industrial-grade films. This difference is likely caused by processing techniques and the overall film's surface quality. However, all PEI films relevant to this study were made in an identical manner, so comparisons among them are appropriate. Comparison of the onset of the probability curves (small FVE radius regime) or the maximum probability FVE radii to the E_{BD} values in Table 1 shows no correlation between the two quantities. However, a comparison of the E_{BD} values to the probability amplitude contained in the large size range tails of the RPD curves shows there is a correlation between FVE sizes and dielectric breakdown fields.

Fig. 4B shows an expanded view of the large FVE region of the three RPD curves shown in panel A that could be tested for the E_{BD}s. *p*-Toluidine-PEI is omitted because it was not possible to measure the breakdown field of this film due to a poor surface quality. 2,4,6-tri-*tert*-Butylaniline-PEI has an RPD distribution with zero probability amplitude beyond 3.35 Å, which out of all samples, has its cutoff for its RPD at the smallest FVE. This is the film with the highest E_{BD}. 4-*tert*-Butylaniline-PEI has a tail in its RPD curve that extends to 3.7 Å and higher amplitude in the large FVE regime compared to the other two curves, as well as the lowest E_{BD}. Meanwhile, the RPD curve for 1-adamantylamine-PEI, which also extends to 3.7 Å, has a smaller integrated amplitude in the tail compared to 4-*tert*-butylaniline-PEI, but larger than 2,4,6-tri-*tert*-butylaniline-PEI, and it has an intermediate E_{BD}. We take the probability at an FVE radius value of 3.4 Å as a reference point to illustrate the differences across films. 2,4,6-tri-*tert*-Butylaniline-PEI has zero probability at this value, followed by 1-adamantylamine-PEI with 0.16, and 4-*tert*-butylaniline-PEI with 0.30.

These observations indicate that, in general, larger FVEs result in lowered E_{BD} values. Additionally, when different films have the same range of FVE radii (1-adamantylamine-PEI vs. 4-*tert*-butylaniline-PEI), it is the integrated probability of having larger radii that is correlated with the E_{BD} strength. It is important to note that the small FVE radius end of the distributions, the curves' maxima or the average FVE radii do not correlate with the measured E_{BD}. A theoretical model that may be consistent with these observations is discussed below.

ROAM does not assume a functional form for polymer films' RPD curves. The non-Gaussian character of the curves is obtained from the analysis through a combination of the absorption line shape and the ROAM-measured frequency-dependent FVE radii. Unlike other techniques that measure FVE sizes, the main reason that a correlation of RPD tail amplitude to breakdown field is possible using ROAM is that RPD curves *can* be highly non-Gaussian. The accuracy and sensitivity of ROAM in measuring RPD curves is fundamental to the observations made in this study.

While the quality of the *p*-toluidine-PEI film was not high enough to perform the dielectric breakdown measurements, its RPD from the ROAM analysis (see Fig. 4A) shows that this film has a probability amplitude in the tail that is greater than 1-adamantylamine-PEI but less than 4-*tert*-butylaniline-PEI. The result suggests that *p*-toluidine-PEI would have an E_{BD} at an intermediate value between 1-adamantylamine-PEI and 4-*tert*-butylaniline-PEI.

All of the results presented above are from variations of a single polymer, so it is informative to examine chemically distinct systems. Fig. 5 shows the FVE RPD curves of PhSeCN in PEI, polystyrene (PS), and poly(methyl methacrylate) (PMMA). For this comparison, PEI purchased from Sigma Aldrich was used, and the procedures for making the film were identical to those presented in the experimental section. This PEI source was preferred for this comparison because it matches that of PMMA and PS films. The results for PS and PMMA have been published before in the context of developing the mathematical formalisms for ROAM [51]. The RPD curves of PEI, PMMA, and PS display maxima at 2.91 Å, 2.94 Å, and 3.30 Å, respectively. The RPD of PEI is essentially Gaussian in shape and spans the range from 2.0 to

TABLE 1

Breakdown field strengths and parameters for RPD curves and FT-IR spectra of end capped polyetherimide films, commercial polyetherimide, poly (methyl methacrylate), and polystyrene.

	Breakdown field (MV/m)	RPD maximum radius (Å)	RPD width (Å)	RPD amplitude at r = 3.4 Å	FT-IR center frequency (cm^{-1})	FT-IR FWHM (cm^{-1})
4-*tert*-Butylaniline-PEI	392 ± 24	2.94 ± 0.01	0.22[a] ± 0.01	0.30	2154.1 ± 0.1	10.4 ± 0.1
1-Adamantylamine-PEI	429 ± 12	2.76 ± 0.01	0.29[a] ± 0.01	0.16	2153.9 ± 0.1	10.6 ± 0.1
2,4,6-tri-*tert*-Butylaniline-PEI	467 ± 22	2.85 ± 0.01	0.15 ± 0.01	0.00	2154.1 ± 0.1	10.4 ± 0.1
p-Toluidine-PEI	–	2.75 ± 0.01	0.29[a] ± 0.01	–	2154.1 ± 0.1	10.5 ± 0.1
Poly(methyl methacrylate)	~446[b]	2.94 ± 0.01	0.31[a] ± 0.01	–	2154.9 ± 0.1[d]	10.5 ± 0.1[d]
Polystyrene	~175[c]	3.30 ± 0.01	0.53[a] ± 0.01	–	2155.4 ± 0.1[d]	8.4 ± 0.1[d]
PEI (commercial)	~500[e]	2.91 ± 0.01	0.27[a] ± 0.01	–	2154.1 ± 0.1	10.8 ± 0.2

– *Measurement not available/relevant to the discussion.*

[a] *Convolution of the standard deviations of two Gaussian functions used to fit the FVE RPD curve.*

[b] Ref. [86].

[c] Ref. [87].

[d] Ref. [51].

[e] Ref. [85].

3.7 Å, whereas PMMA and PS have non-Gaussian distributions, spanning the range from 2.25 Å to 3.9 Å, and from 2.6 to 5.0 Å, respectively. Values of E_{BD} vary in the literature, but there seems to be consensus that the breakdown field of PEI is the highest (~500 MV/m), followed by PMMA (~446 MV/m), and then by PS (~175 MV/m) [34,85–87]. As seen in the results presented above, the polymer with the highest E_{BD}, PEI, also has its RPD curve go to zero at the smallest radius. PEI is followed in order of decreasing E_{BD} by PMMA, which displays a small tail to large FVE radii, and then by PS, which has both the lowest E_{BD} and a long tail to large radii, giving it larger FVEs than both PEI and PMMA. These observations are in accord with the observations made with the end capped PEI films.

A model of electron acceleration inside polymer FVEs was proposed by Artbauer in 1996 [42]. In this model, electrons are dislodged from the polymer by the ionization of thermally activated centers, providing free electrons as charge carriers in the dielectric breakdown process. The concentration of charge carriers depends on the ionization energy, E_i, of the polymer, the temperature, T, of the system, and the strength of the external electric field, F.

Artbauer proposed that a free electron of charge e, located inside an FVE is accelerated by an external electric field, F, across a free path, x, which corresponds to the size of the FVE in the direction of the field. Acceleration in directions other than the field direction is taken to be negligible and ignored. By the time the electron reaches the opposite end of the FVE, it has gained energy $E_e = eFx$. At the end of the FVE, the electron encounters an energy barrier, E_μ, imposed by the polymer wall, which controls the probability that the electron will be able to escape the initial FVE and move to an adjacent FVE. If the electron has enough energy to escape, it can go on to eject other electrons, which can result in a cascading effect, with more and more electrons accelerated by the external electric field, thus causing current flow.

The probability of electron escaping an FVE is given by [42],

$$P_\mu = e^{\frac{-(E_\mu - eF\ x)}{kT}} \tag{6}$$

where k is the Boltzmann constant, and T is the temperature in degrees Kelvin. The current density is given by,

$$i = n_e e v \tag{7}$$

where n_e is the number of charge carriers, e is the charge of the electron, and v is the mean velocity of the electron at the energy barrier. The Joule losses, which are proportional to the current density, also increase. This process generates local heating, and as the current flow increases, the heat generated cannot be fully dissipated. Eventually, a filamentary local thermal breakdown develops along the path that connects the two surfaces at which the external field is applied. This process creates a current path, resulting in dielectric breakdown. In terms of the free path for acceleration, breakdown occurs when the following condition is met,

$$Fx = E_\mu / e \tag{8}$$

because at this value of Fx the escape probability is 1 (Eq. (6)). Therefore, electrons found in long free path FVEs will have the best chance of moving from one FVE to another due to acceleration. In this theory, dielectric breakdown results from the largest free paths in the film, which corresponds to its largest FVEs. Additionally, since the current density (Eq. (7)) is proportional to the number of charge carriers, breakdown also depends on the number of the largest FVEs. This model takes the FVEs to have an ellipsoidal shape, and acceleration is understood to occur along the long axis.

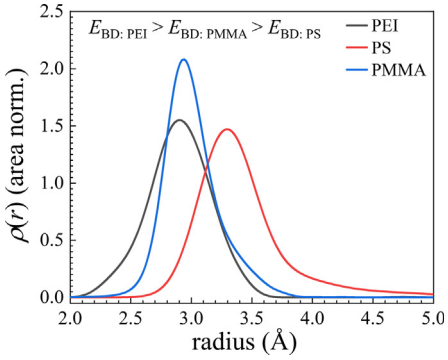

FIG. 5

FVE radii probability distribution curves for PEI, PMMA, and PS. The FVE radius probability distribution curves for PMMA and PS are non-Gaussian, with tails to large FVE radii. The probability amplitude contained in the large radius range is inversely correlated with the films' breakdown fields (obtained from the literature).

ROAM measures the radius of FVEs. The model is discussed in terms of the probe being in a cylinder, but the measured radii are independent of the actual shape. However, the probe will be stopped by the nearest surface encountered as reorientation occurs about the center of mass. In an ellipsoidal cavity, the ROAM radius would be the short axis. Artbauer presents an argument in which the short and long axes of the ellipsoid are proportional to one another; thus, a wider elliptical FVE (larger FVE radius from ROAM) would also provide a longer acceleration path. The electron acceleration model estimates the acceleration path along the long axis of the ellipsoid needed for breakdown in PMMA as ~12 Å, which is less than twice the larger diameters (~7 Å) measured by ROAM (Fig. 5A), but within a reasonable range when considering that the ROAM radius corresponds most closely with the short axis of the ellipsoids in Artbauer's model.

Although there are only 3 polymers, the RPD curves presented in Fig. 4 are in accord with the Artbauer model. Our results show that the polymer with the smallest extension of its RPD to large radii also has the highest E_{BD}. While the polymers that have FVE tails to large radii, have E_{BD}s that decrease as the probability in the tails increases. Other aspects of the RPD curves do not correlate with the measured E_{BD}s. In terms of the Artbauer model, breakdown fields are determined by a film's large FVEs.

Finally, the top x-axis of Fig. 1 gives the electric fields experienced by the vibrational probe inside FVEs in the PEI films as determined from analysis using first order Stark spectroscopy [76]. In terms of the first order Stark effect, the frequency of a vibrational mode is determined by the electric field it experiences plus a zero field contribution as follows:

$$\omega = \omega_0 + \mu E \tag{9}$$

where ω_0 is the zero-field vibrational frequency with a value of 2163.7 cm^{-1} and μ is the Stark tuning rate with a value of

12.3 cm^{-1}/(GV/m) [76]. Both of these parameters were determined for PhSeCN by a calibration that involves measuring the CN absorption spectrum in 10 solvents [76,88]. The electric field, *E*, is determined using the Onsager cavity model. The procedure is well established and has been used routinely in many contexts including a variety of nitriles [88]. In some instances, there is evidence that a purely first order Stark model does not completely capture all the intricacies of the vibrational frequency shifts, especially when the *E*-field magnitudes become very large and when a large variety of chemical environments are compared. However, given that the measured frequencies are being observed in almost identical chemical systems with *E*-field magnitudes on the smaller side of those experienced in molecular solvents, the results presented in Fig. 1 are expected to provide good estimates of the fields present inside PEI FVEs.

The resulting *E*-field magnitudes span a very wide range, which includes the measured breakdown fields shown in Table 1. The FVEs are aligned in random directions relative to an applied external field. Therefore, polymer induced internal FVE *E*-fields can add to or subtract from the applied *E*-field. A strong applied external field will produce some shift in the configuration of side groups and possibly small chain segments. Such changes will influence the magnitude and direction of the polymer generated electric fields inside the FVEs. None of these considerations are included in the Artbauer theory, and it is unknown what role, if any, the polymer generated *E*-fields internal to the FVEs play in the breakdown process. The *E*-fields and the correlation of *E*-field with FVE size are observables from the ROAM experiments, which may be useful in understanding dielectric breakdown.

Concluding remarks

We have used a combination of synthetic organic chemistry, ultrafast infrared laser spectroscopy, and dielectric measurements to investigate the relationship among polymer structures, FVE radius probability distributions, and dielectric breakdown fields. We synthetically modified polyetherimide, an important dielectric material, to have a variety of small organic molecules as end-groups. ROAM was used to obtain the FVE radius probability distribution of each polymer, and their dielectric breakdown fields were measured.

An important result is that the synthetic modification of PEI, which only changed the end groups, had substantial impact on the RPDs, at least for these relatively short chains of ~40 monomers. For long chains, it is likely that the RPD is modified in the vicinity of the end group. The range of modifications probably extends distances corresponding to at least several tens of monomer units. Fig. 4 shows the RPDs for the four polymers studied. Both the centers of the distributions and shapes of the distribution change substantially as the end groups are changed. The results show that a small synthetic modification, which leaves the bulk of the molecular structure unchanged, has a significant impact on the polymer chain packing in the film.

It was observed that the FVE sizes and breakdown fields are correlated. The film with the FVE RPD that cuts off at the smallest size displayed the highest breakdown field. The breakdown field decreased with increasing probability of having large FVEs, i.e., tails of the distributions to large radii. There were no correlations between breakdown fields and the FVE small size range, the RPD curve maximum, or the average FVE radius. The results indicate that a polymer film's breakdown field for a set of polymers with the same main chain is related to the probability of having large FVEs.

The correlation between breakdown field and large FVEs are in accord with Artbauer's theory of electron acceleration inside FVEs. Small FVEs, which result from improved polymer chain packing, provide a short free path length for electron acceleration by an applied external electric field. Short acceleration distances do not provide charge carriers with enough energy to have a high escape probability, i.e., able to penetrate the FVE wall to reach another FVE. In the Artbauer model, transit from one FVE to another generates a high current density, which leads to dielectric breakdown.

Our results highlight that it is not necessary to introduce large structural modifications to a polymer (branching, cross-linking, or co-polymerization) to modify its distribution of free volume element sizes for relatively short chains. Changing the end groups provides a synthetic framework to introduce small systematic modifications that leave the underlying electronic structure of the material unchanged. This approach enabled a controlled comparison of polymer films' FVE size distributions and breakdown characteristics.

This study provides experimental evidence that there is a mechanistic link between having large FVE sizes including tails to large size of the FVE radius probability distribution in a polymer film and its breakdown field. The results suggest that to create a dielectric film with a high breakdown field, the synthesis and processing should target the creation of the most efficient chain packing to reduce the probability of large FVEs. The results also have implications for extrinsic breakdown. It is possible that long-term exposure of a polymer film to high electric fields will result in structural changes that produce larger FVEs. The results presented here indicate that production of larger FVEs would lower the E_{BD}, resulting in breakdown at the same electric fields that did not initially result in breakdown. This hypothesis can be tested through studies that combine electric field aging and ROAM measurements of changes in the RPDs.

CRediT authorship contribution statement

Sebastian M. Fica-Contreras: Conceptualization, Methodology, Software, Validation, Formal analysis, Data curation, Investigation, Writing – original draft, Writing – review & editing, Visualization. **Zongze Li:** Investigation, Formal analysis. **Abdullah Alamri:** Investigation, Validation, Formal analysis. **Aaron P. Charnay:** Validation, Investigation. **Junkun Pan:** Validation. **Chao Wu:** Investigation. **Jeffrey R. Lockwood:** Investigation. **Omer Yassin:** Investigation. **Stuti Shukla:** Investigation. **Gregory Sotzing:** Conceptualization, Methodology, Formal analysis, Supervision, Funding acquisition, Project administration. **Yang Cao:** Conceptualization, Methodology, Formal analysis, Supervision, Writing – review & editing, Funding acquisition, Project administration. **Michael D. Fayer:** Conceptualization, Methodology, Formal analysis, Supervision, Writing – original draft, Writing – review & editing, Funding acquisition, Project administration.

Data availability

Data will be made available on request.

Declaration of Competing Interest

The authors declare that they have no known competing financial interests or personal relationships that could have appeared to influence the work reported in this paper.

Acknowledgements

This work was supported by Office of Naval Research Grant N00014-17-1-2656.

Data availability

The raw/processed data required to reproduce these findings cannot be shared at this time due to technical or time limitations.

Appendix A. Supplementary material

Supplementary material contains Organic synthesis of end capped PEI; NMR spectra of PEI films; Gel permeation chromatography (GPC); Thermal characterization (TGA and DSC); Dielectric constant determination; Drying polymer films; FT-IR spectroscopy of PhSeCN in PEI films; Orientational dynamics of PhSeCN in PEI films; RPD curve extraction; and Breakdown field measurements. Supplementary material to this article can be found online at https://doi.org/10.1016/j.mattod.2023.05.010.

References

[1] R. Greiner, F.R. Schwarzl, Rheol. Acta 23 (1984) 378–395.
[2] W.G. Knauss, I.J. Emri, Comput. Struct. 13 (1981) 123–128.
[3] K.M. O'Connor, K.M. Scholsky, Polymer 30 (1989) 461–466.
[4] Z.X. Low et al., Chem. Rev. 118 (2018) 5871–5911.
[5] M.H. Cohen, D. Turnbull, J. Chem. Phys. 31 (1959) 1164–1169.
[6] D. Turnbull, M.H. Cohen, J. Chem. Phys. 34 (1961) 120–125.
[7] R.P. White, J.E.G. Lipson, ACS Macro Lett. 4 (2015) 588–592.
[8] R.P. White, J.E.G. Lipson, Macromolecules 49 (2016) 3987–4007.
[9] B.R. Wilks et al., J. Polym. Sci. B Polym. Phys. 41 (2003) 2185–2199.
[10] S.K. Sharma et al., RSC Adv. 6 (2016) 67997–68004.
[11] R.E. Robertson, Macromolecules 18 (1985) 953–958.
[12] Y.P. Yampolskii, Russ. Chem. Rev. 76 (2007) 59–78.
[13] J.C. Jansen et al., Macromolecules 42 (2009) 7589–7604.
[14] J.Y. Park, D.R. Paul, J. Membr. Sci. 125 (1997) 23–39.
[15] I.A. Ronova et al., Macromol. Theory Simul. 12 (2003) 425–439.
[16] D. Hofmann et al., Macromolecules 36 (2003) 8528–8538.
[17] V.P. Shantarovich et al., Phys. Stat. Sol. (c) 4 (2007) 3776–3779.
[18] B. Fan et al., Prog. Polym. Sci. 97 (2019) 101143.
[19] J.S. Ho, S.G. Greenbaum, ACS Appl. Mater. Interfaces 10 (2018) 29189–29218.
[20] D.H. Wang et al., Polym. Chem. 53 (2015) 422–436.
[21] P. Singh et al., J. Alloys Compd. 648 (2015) 698–705.
[22] B. Luo et al., J. Mater. Chem. A 2 (2014) 510–519.
[23] T. Yamada, T. Ueda, T. Kitayama, J. App. Phys. 53 (1982) 4328–4332.
[24] D. Xu et al., Macromol. Mater. Eng. 305 (2020) 1900820.
[25] R. Ma et al., ACS Appl. Mater. Interfaces 6 (2014) 10445–10451.
[26] Y. Wang et al., IEEE Trans. Dielectr. Electr. Insul. 17 (2010) 1036–1042.
[27] C. Kim, G. Pilania, R. Ramprasad, Chem. Mater. 28 (2016) 1304–1311.
[28] Y. Sun et al., IEEE Electr. Insul. Mag. 29 (2013) 8–15.
[29] V.A. Zakrevskii, N.T. Sudar, Phys. Solid State 55 (2013) 1395–1400.
[30] S.R. Forrest, Nature 428 (2004) 911–918.
[31] J.H. Cho et al., Nat. Mater. 7 (2008) 900–906.
[32] M. Kaltenbrunner et al., Nature 499 (2013) 458–463.
[33] B. Zhang et al., Adv. Mater. 33 (2021) 2101374–2101380.
[34] C.A. Grabowski et al., Nanocomposites 2 (2016) 117–124.
[35] M. Ieda, IEEE Trans. Dielectr. Electr. Insul. EI-15 (1980) 206–224.
[36] S. Lombardo et al., J. Appl. Phys. 98 (2005) 121301.
[37] V.A. Zakrevskii, V.A. Pakhotin, N.T. Sudar, J. Appl. Phys. 115 (2014) 234101.
[38] T. Takada et al., IEEE Trans. Dielectr. Electr. Insul. 22 (2015) 1240–1249.
[39] S. Kim et al., Sci. Technol. Adv. Mater. 19 (2018) 486–494.
[40] C.G. Hardy et al., Chem. Mater. 25 (2013) 799–807.
[41] X. Yuan, T.C.M. Chung, Appl. Phys. Lett. 98 (2011) 062901.
[42] J. Artbauer, J. Phys. D: Appl. Phys. 29 (1996) 446–456.
[43] V.A. Kusuma et al., Polymer 180 (2019) 121666.
[44] Q.M. Jia et al., Eur. Polym. J. 43 (2007) 35–42.
[45] D. Bamford et al., Macromol. Chem. Phys. 207 (2006) 492–502.
[46] R.Y.F. Liu et al., J. Appl. Polym. Sci. 98 (2005) 1615–1628.
[47] V.A. Kusuma et al., J. Membr. Sci. 359 (2010) 25–36.
[48] T.-T. Hsieh, C. Tiu, G.P. Simon, J. Appl. Polym. Sci. 82 (2001) 2252–2267.
[49] J.C. Sworen et al., J. Am. Chem. Soc. 126 (2004) 11238–11246.
[50] G. Dlubek et al., Macromol. Chem. Phys. 205 (2004) 512–522.
[51] S.M. Fica-Contreras et al., J. Am. Chem. Soc. 143 (2021) 3583–3594.
[52] G. Sui et al., Soft Matter 5 (2009) 3593–3598.
[53] B.-K. Chen, J.-U. Du, C.-W. Hou, IEEE Trans. Dielectr. Electr. Insul. 15 (2008) 127–133.
[54] R. Ramani et al., J. Phys. Chem. B 118 (2014) 12282–12296.
[55] N. Pfeiffenberger et al., IEEE Trans. Dielectr. Electr. Insul. 25 (2018) 120–126.
[56] B.-K. Chen et al., Polym. Bull. 57 (2006) 671–681.
[57] B.-K. Chen, Y.-T. Fang, J.-R. Cheng, Macromol. Chem. Phys 242 (2006) 34–39.
[58] C. Wu et al., Adv. Mater. 32 (2020) 2000499–2000504.
[59] A. Alamri et al., Chem. Mater. 34 (2022) 6553–6558.
[60] S.A. Benchérif et al., Acta Biomater. 5 (2009) 1872–1883.
[61] Q. Zhang et al., Macromolecules 41 (2008) 536–538.
[62] L. Yuan, M. Ji, S. Yang, J. Appl. Polym. Sci. 134 (2017) 45168.
[63] T. Miyashita et al., Angew. Chem. Int. Ed. Engl. 56 (2017) 5288–5293.
[64] S.B. Mhaske et al., J. Appl. Polym. Sci. 77 (2000) 627–635.
[65] L. Xu et al., Des. Monomers Polym. 21 (2018) 99–104.
[66] H. Jia et al., High Perform. Polym. 34 (2022) 1143–1151.
[67] B. Kost et al., Prog. Polym. Sci. 130 (2022).
[68] C. Yan et al., J. Am. Chem. Soc. 139 (2017) 16518–16527.
[69] S.K. Karthick Kumar, A. Tamimi, M.D. Fayer, J. Chem. Phys. 137 (2012) 184201.
[70] D.J. Hoffman et al., J. Chem. Phys. 153 (2020) 204201.
[71] H.-S. Tan, I.R. Piletic, M.D. Fayer, J. Opt. Soc. Am. B 22 (2005) 2009–2017.
[72] A. Tokmakoff, J. Chem. Phys. 105 (1996) 1–12.
[73] H.S. Tan, I.R. Piletic, M.D. Fayer, J. Chem. Phys. 122 (2005) 174501.
[74] G. Lipari, A. Szabo, Biophys. J. 30 (1980) 489–506.
[75] G. Lipari, A. Szabo, J. Am. Chem. Soc. 104 (1982) 4546–4559.
[76] D.J. Hoffman, S.M. Fica-Contreras, M.D. Fayer, Proc. Natl. Acad. Sci. U.S.A. 117 (2020) 13949–13958.
[77] A. Tokmakoff, M.D. Fayer, J. Chem. Phys. 103 (1995) 2810–2826.
[78] D.E. Moilanen et al., Proc. Natl. Acad. Sci. U.S.A. 106 (2009) 375–380.
[79] D.J. Hoffman, K.P. Sokolowsky, M.D. Fayer, J. Chem. Phys. 146 (2017) 124505.
[80] Y.C. Jean et al., Macromolecules 46 (2013) 7133–7145.
[81] J. Liu, Q. Deng, Y.C. Jean, Macromolecules 26 (1993) 7149–7155.
[82] H.-L. Li et al., Polymer 40 (1999) 349–355.
[83] M. Ban et al., J. Polym. Sci. B Polym. Phys. 34 (1996) 1189–1195.
[84] Z.P. Madzarevic et al., Macromolecules 51 (2018) 9925–9932.
[85] J. Ho, R. Jow, Laboratory (2009).
[86] Q. Chi et al., J. Mater. Chem. C 7 (2019) 14148–14158.
[87] V.K. Thakur et al., Polym. Chem. 2 (2011) 2000–2009.
[88] N.M. Levinson, S.D. Fried, S.G. Boxer, J. Phys. Chem. B 116 (2012) 10470–10476.